Chemical Synthesis and Structural Characterization of Highly Disordered Ni Colloidal Nanoparticles

Herbert Winnischofer,[†,§] Tulio C. R. Rocha,[†,‡] Wallace C. Nunes,[‡] Leandro M. Socolovsky,[‡] Marcelo Knobel,[‡] and Daniela Zanchet[†,*]

[†]LNLS-Brazilian Synchrotron Light Laboratory, C.P. 6192, Campinas, SP, 13083-970, Brazil, and [‡]Instituto de Física "Gleb Wataghin", Universidade Estadual de Campinas, C.P. 6165, Campinas, SP, 13083-970, Brazil. [§]Present address: Departamento de Química, Setor de Ciências Exatas, Universidade Federal do Paraná, C.P.19081, Curitiba, PR, 81531-990, Brazil.

ABSTRACT This work focuses on synthetic methods to produce monodisperse Ni colloidal nanoparticles (NPs), in the 4−16 nm size range, and their structural characterization. Narrow size distribution nanoparticles were obtained by high-temperature reduction of a nickel salt and the production of tunable sizes of the Ni NPs was improved compared to other methods previously described. The as-synthesized nanoparticles exhibited spherical shape and highly disordered structure, as it could be assigned by X-ray diffraction (XRD) and high resolution transmission electron microscopy (HRTEM). Annealing at high temperature in organic solvent resulted in an increase of nanoparticle atomic ordering; in this case, the XRD pattern showed an fcc-like structure. Complementary data obtained by X-ray absorption spectroscopy confirmed the complex structure of these nanoparticles. Temperature dependence of the magnetic susceptibility of these highly disordered Ni NPs showed the magnetic behavior cannot be described by the conventional superparamagnetic theory, claiming the importance of the internal structure in the magnetic behavior of such nanomaterials.

KEYWORDS: nanoparticle · crystal structure · nickel · magnetic properties

Nanostructured materials have been extensively explored for the fundamental scientific and technological interests in accessing new classes of functional materials with unprecedented properties and applications.[1−3] In this class of system, the size and shape of the nanostructure mainly determines electric, optic, magnetic, and catalytic properties. Therefore, synthetic methodologies that provide routes to obtain nanostructures in a predictable, controllable, and reproducible way have become an important issue. The synthetic procedures to obtain highly homogeneous colloidal nanoparticles (NPs), in particular, have already been established for several systems, and some recent reviews in this area can be pointed out.[4−7] For example, Park *et al.*[8] recently described an interesting strategy to produce one-nanometer-scale size-controlled samples of Fe_3O_4 NPs.

Nickel is one of the transition metals that exhibit magnetism as bulk material and other interesting properties and applications, such as in hydrogen storage and catalysis. Methods to produce Ni NPs can be found in the literature and involve high-temperature organometallic decomposition,[9,10] electrochemical reduction,[11] or chemical reduction.[12,13] However, many factors that affect the mean size of the Ni NPs or their size distribution have not been extensively addressed in the literature. Since the properties of nanometric materials are deeply affected by the mean size and the size distribution of the particles, it is very important to address which are the factors that rule those characteristics. In addition, a detailed description of a robust and reproducible way to prepare Ni NPs will find interest in many research fields, such as chemistry, physics, biology, catalysis, and materials science. In this work, we describe in detail the chemical synthesis of Ni NPs in the 4−16 nm range and discuss some aspects that affect the mean size and size distribution. The synthetic procedures described here were based on the chemical reduction of nickel salts ($Ni(CH_3COO)_2$ or $Ni(acac)_2$ (acac = acetylacetonate), and were adapted from the work previously described by Murray *et al.*[14,15] and Son *et al.*,[16] extending these methods to prepare Ni NPs with six different mean sizes. The Ni NPs morphology and structure were characterized by transmission electron microscopy (TEM) at conventional and at high resolution mode (HRTEM), small-angle X-ray scattering (SAXS), X-ray diffraction (XRD), X-ray photoelectron spectroscopy (XPS), and X-ray absorption near-edge structure spectroscopy (XANES). Temperature dependence of the magnetic susceptibility of these Ni NPs was also addressed in this work.

*Address correspondence to zanchet@lnls.br.

Received for review August 8, 2007 and accepted April 28, 2008.

Published online May 21, 2008.
10.1021/nn700152w CCC: $40.75

TABLE 1. Experimental Conditions Used To Synthesize Ni Colloidal NPs

sample	counterion	ligands	molar ratio to Ni^{2+}	T (°C)[a]	average size (nm)
Ni1	acetate	oleic acid	1	200	4.8 ± 0.4
		n-trioctylamine	4		
		n-trioctylphosphine	2		
Ni2	acetate	oleic acid	1	215	7.5 ± 0.7
		n-trioctylamine	2		
		n-trioctylphosphine	1		
Ni3	acetate	oleic acid	1	250	11.7 ± 0.5
		n-tributylamine	2		
		n-tributylphosphine	1		
Ni4	acetylacetonate	oleic acid	1	250	8.8 ± 0.6
		n-trioctylamine	4		
		n-trioctylphosphine	2		
Ni5	acetylacetonate	oleic acid	1	250	12.8 ± 0.7
		n-oleylamine	4		
		n-trioctylphosphine	2		
Ni6	acetylacetonate	oleic acid	1	250	16.3 ± 0.4
		n-trioctylamine	2		
		n-trioctylphosphine	1		
Ni7 (= Ni2 annealed)				230	8.7 ± 1.4
Ni8	acetylacetonate	oleylamine	37	215	7.8 ± 0.7
		n-trioctylphosphine	9		

[a]The temperatures are the boiling points of the corresponding reaction mixtures.

RESULTS AND DISCUSSION

Size and Growth. Table 1 presents a summary of the reaction conditions used in this work. The variables were the molar ratio of ligands to nickel salt (Ni1 and Ni2), ligands type (Ni2 and Ni3, Ni4 and Ni5) and type of nickel salt (Ni4 and Ni6; compare with Ni1 and Ni2). It is important to remark that the reaction temperatures provided are the boiling temperatures of the synthesis solution; in this aspect this is a fixed parameter in all the synthesis. In this type of synthesis, a better control is usually achieved by synthesizing at the boiling temperature. Ni7 sample was produced by a postsynthesis annealing of the Ni2 sample, aiming to address its influence in the atomic order of the NPs. Ni8 was produced by a different method (see Experimental Section), and we did not intend to compare the synthesis conditions with the others; the aim was only to compare the final characteristics of the NPs.

Figure 1 shows some representative TEM images from samples Ni1 to Ni6. The corresponding size distribution histograms are presented in the Supporting Information (Figure S1, Supporting Information). In general, Ni NPs exhibit spherical shape, but faceting can be seen in some particles. We can verify an increase in the mean diameter from Ni1 to Ni3 and Ni4 to Ni6, depending on the Ni precursor. All samples show a narrow size distribution, especially those obtained using $Ni(acac)_2$ precursor (Figure 1D−F). These results were confirmed by SAXS, which showed the typical oscillations found for spherical particles with narrow size distribution (SAXS results are shown in Figure S2, see Supporting Information). The NPs growth is kinetically controlled, thus the reaction temperature could play a crucial role in their size control and we chose to keep it at the boiling point for all reactions. For the smaller NPs, Ni1 and Ni2, the reactions were conducted at lower temperatures, 200 and 215 °C, respectively, since for

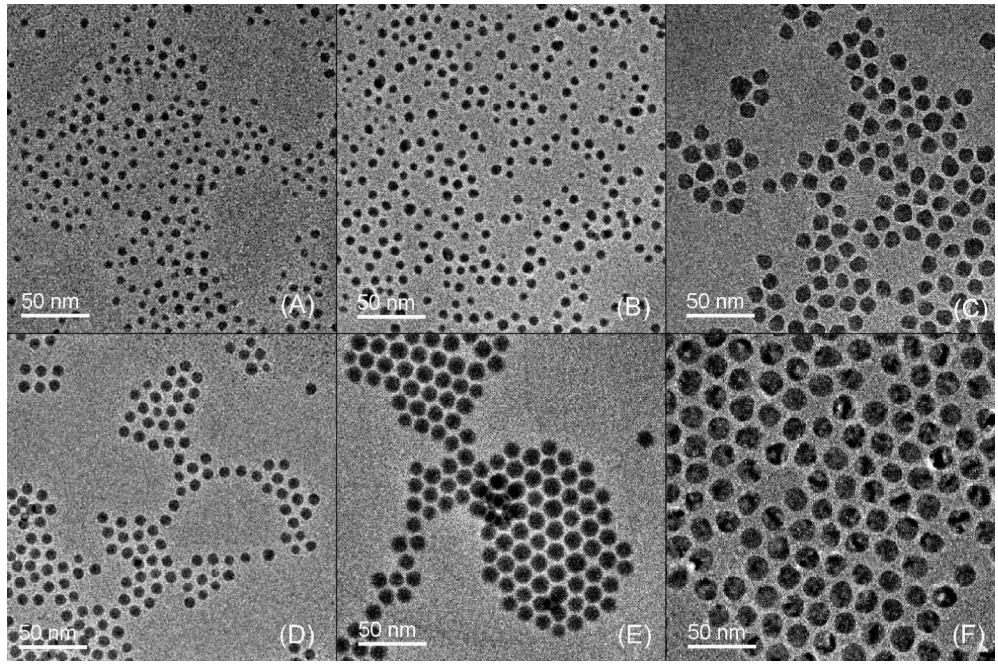

Figure 1. TEM images from Ni NP samples (A) Ni1, (B) Ni 2, (C), Ni 3, (D) Ni 4, (E) Ni 5, and (F) Ni 6.

these two reactions it was not possible to further increase the temperature because of the mixture boiling. The lower temperature plateaus for these two reaction mixtures may be due to the high ligand concentration and the use of acetate salt (the decomposition of acetate salt occurs at lower temperatures than the acetylacetonate (unpublished results)). For other NP reactions, the temperatures could be increased up to 250 °C.

From Ni1 to Ni3 and Ni4 to Ni6 we can observe the roles of the ligand type and their molar ratio to Ni^{2+} in the final size of the NPs. The influence of the ligands can be understood by considering the La Mer mechanism.[17] This mechanism is based on a saturated solution that causes the nucleation of the NPs that behave as seeds to the subsequent growth. The NP growth depends on the adsorption of ions on the seeds surface and reduction and this crucial step for size control is diffusionally limited. Ligands with larger carbonic tails cause a steric hindrance in the ions adsorption and as result, smaller NPs are produced. In a similar way, with an increase in the ligand molar ratio to the Ni^{2+}, a better surface stabilization of the seeds and a more difficult growth is expected.

The analysis of Table 1 also points out that the counterion of the salt precursor plays an important role not only in the solubility of the salt in the organic solvent but also by affecting the mean size and size distribution of the produced NPs. As we observe in the TEM images, the substitution of $Ni(CH_3COO)_2$ by $Ni(acac)_2$ lead to larger NPs and narrower size distributions (Table 1). Therefore, the role of the counterion seems to be related to the formation of different intermediates at the nucleation step. It is known that counterions such as acetate or acetylacetonate form polynuclear complexes[18,19] that may contribute to the nucleation of the particles. In fact, at dry conditions the complex "Ni acac" is not $Ni(acac)_2$ but the trimer ($[Ni(acac)_2]_3$) (see for example references 20 and 21). The polinuclear complexes formed at high temperatures by acetylacetonate may lead to a faster growth process, resulting in larger NPs.

The analysis of TEM image contrast within each NP may also provide qualitative information about NP crystallinity. In the case of the Ni6 sample (Figure 1F), the contrast variation within each NP is clear, showing that they are formed by more than one crystalline domain (*i.e.*, the NPs are not single crystals). This observation was supported by the broad XRD patterns of all samples and HRTEM images (see discussion later). Interesting, in the annealing experiment (Ni2 and Ni7 samples) we verified an improvement of the atomic order, despite the increase of the size distribution, from 8.6% (Ni2) to 17% (Ni7), and the average size, from 7.5 to 8.6 nm, respectively (see Figure S3). The mechanism that affects the average size and size distribution during annealing has not been completely understood yet, but it may suggest that Ostwald ripening takes place, where small particles are consumed as the larger NPs grow.

Structural Characterization. Ni NPs prepared by chemical reduction in organic medium have been previously described either as amorphous[22] or as fcc-like (face-centered-cubic),[14,22,23] based on the broad peak at $s = 0.45-0.50$ Å^{-1} in the XRD patterns (s is the modulus of the scattering vector and is equal to $2 \sin \theta/\lambda$). The formation of a highly disorder structure and its origin has not been addressed in detail in previous works.[14,22,23] It is interesting to note that other authors have reported variable results for Ni NPs prepared in different conditions. Couto *et al.*[24] prepared Ni NPs in ethylene glycol using sodium borohydride as a reducing agent in the presence of poly(*N*-vinilpyrrolidone). In this case, the XRD curves also present broad peaks that point to an fcc-like structure. Chen *et al.*[25] obtained highly crystalline fcc Ni NPs (~10 nm) by reduction of Ni^{2+} by hydrazine in the presence of cetyltrimethylammonium bromide and traces of NaOH in aqueous media. Jeon *et al.*[26] reduced Ni^{2+} using hydrazine dissolved in tetrahydrofuran and oleylamine as protecting agent. Depending on the temperature that the Ni^{2+} salt was injected into the hydrazine solution the NP samples exhibited only hcp or hcp and fcc diffraction peaks. It is clear that in the case of Ni NPs, the synthesis conditions impact strongly in the atomic structure and as a consequence, in their macroscopic properties, such as the magnetic behavior, as discussed below. The understanding of what determines the atomic arrangement of Ni NPs and other transition metals, such as Co, is a challenge to overcome, and deeper analyses are still required.

In our work, all Ni NPs samples exhibited very broad XRD patterns, similar to that shown in Figure 2A (see also Figure S4). Although the intense peak at $s = 0.49$ Å^{-1} could be assigned to the fcc 111 reflection, there is no clear evidence of the 200 peak, and the broad peak at $s > 0.85$ Å^{-1} could be hardly attributed to the fcc 220 reflection since its value is much larger than the bulk value, 0.8 Å^{-1}. HRTEM images of Ni2 sample (Figure 3A) revealed that the internal structure is not completely amorphous, but instead each NP appears to be formed by very small crystalline regions (size of about 1 nm), where 111 lattice fringes (A) oriented in different directions can be seen (this is the only crystallographic planes that can be normally imaged in our HRTEM). This is in agreement with the broad features observed in Figure 2A.

One exception was the Ni8 sample that exhibited a slightly better resolved XRD profile, with distinguishable 200 and 220 reflections (data shown in Figure S4). However, this sample was prepared by a distinct synthetic route, where the nickel salt was previously dissolved in trioctylphosphine and reaction proceeds with a large excess of ligand oleylamine (see Table 1). It is important to mention that the XRD curve in the original

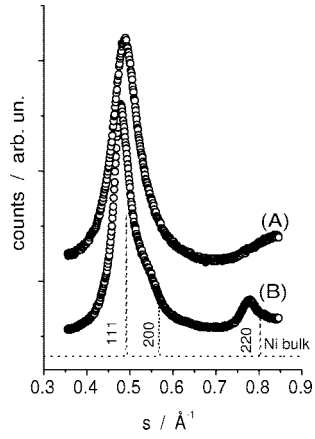

Figure 2. Representative XRD patterns of Ni NP samples (A) Ni2 sample (as-synthesized) and (B) after annealing (Ni7 sample). The dashed line corresponds to the position of Ni fcc bulk peaks and the Miller indices are indicated. (s = 2 sin θ/λ).

work[16] using this procedure is more similar to the broad curves of Ni1−Ni6 than the results we found. The synthetic factors that control the internal structure of the Ni NPs produced by this method and its reproducibility are still unclear at this moment.

In an attempt to improve the crystallinity of the Ni NPs and obtain further insight about this important characteristic, an annealing treatment was performed in Ni2 sample, leading to the Ni7 sample. The XRD pattern of Ni7 (2B) shows an improvement of the atomic order toward the fcc structure, where the 200 peak appears at 0.53 Å^{-1} as a shoulder of the 111 peak and the 220 peak appears at 0.77 Å^{-1}. The increase in crystallinity was confirmed by HRTEM, as can be seen in Figure 3B. The lattice fringes identified in the images are also consistent with the 111 planes of a fcc structure, with 2.1 Å periodicity. The several defects that still persist are

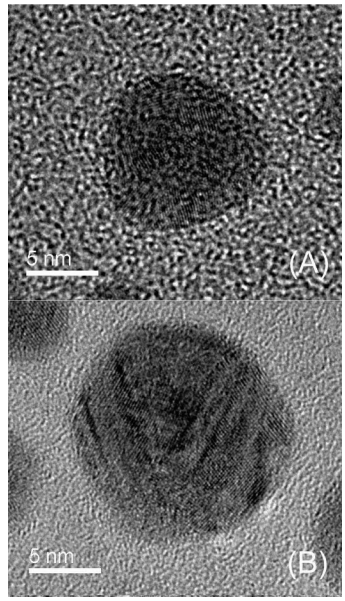

Figure 3. Representative HRTEM images of Ni NPs: (A) Ni2 sample and (B) after annealing (Ni7 sample).

in excellent correspondence to the broadness showed in the XRD pattern. Although we expected that the annealing process would shift the reflections toward the Ni fcc values, the reverse was observed. The 111 and 220 reflection shifts from an fcc position for the as-synthesized (Ni2) sample to a lower value of s for the annealed one (Ni7). The shift to lower values of s in the 111 and 220 peaks could be related to the presence of multiply twinned particles, such as icosahedra (see Supporting Information for the simulated diffraction patterns).[27−29] We further increased the temperature up to 300 °C and time of treatment up to 24 h, but even after 24 h no further improvement in the crystallinity was obtained. The diffraction pattern of the N1 to N6 samples are very similar to the as-synthesized Ni2 sample, and the position of the 111 reflection are close to s = 0.49 Å^{-1}. The XRD curves and the 111 reflection values are summarized in the Supporting Information Table S1.

Surface and Local Structure. The surface composition of NPs obtained by chemical methods may differ from others, since the NPs are capped by ligands that prevent coalescence. Hence, XPS can provide important information of the Ni NPs surface composition. The analysis, performed in the 0−1000 eV binding energy range, showed that the Ni samples have a clean surface with only Ni, C, O, and N elements. Figure 4 shows the results for the Ni1 sample (the other samples showed similar results). The 840−900 eV region (Figure 4A) that comprises the doublet of Ni $2p_{1/2}$ and $2p_{3/2}$ transitions was analyzed. In the Ni $2p_{3/2}$ region, we observed two main peaks at binding energy (BE) of 857 eV (91%) and 854 eV (9%) that could be assigned to $Ni(OH)_2$ and NiO species, respectively. The lower intensity peak at 863 eV, shifted 6 eV from the $Ni(OH)_2$ peak, corresponds to a satellite peak.[30] The same pattern is observed in the Ni $2p_{1/2}$ region (Figure 4A). Also, it is worth noting the lack of significant percentage of metallic Ni species (BE($2p_{3/2}$) = 855 eV)[31] on the NP surface. Couto *et al.*[24] observed a similar result in colloidal Ni NPs produced in a different way. As the XRD data and TEM did not point out the presence of nickel oxide or hydroxide particles or a core−shell structure (metal-oxide), the XPS results indicate the existence of a disordered arrangement of a few atomic layers of Ni^{2+} species on NPs surface. It is interesting to mention, however, that the O 1s transition region (Figure 4B) does not correspond to an oxide or hydroxide species. Only one symmetric peak at 533 eV (fwhm = 3 eV) was identified whose BE could correspond to either O from adsorbed water or carboxylic acid species. Since the samples were carefully washed by ethanol and dried, the excess of ligands, water, and the precursor $Ni(CH_3COO)_2$ salt should have been mostly removed. Nevertheless, despite the narrow and symmetric XPS O 1s peak we cannot completely rule out the possibility of minor contributions of these species to the observed peak.[32] Consequently, the XPS results indicate a

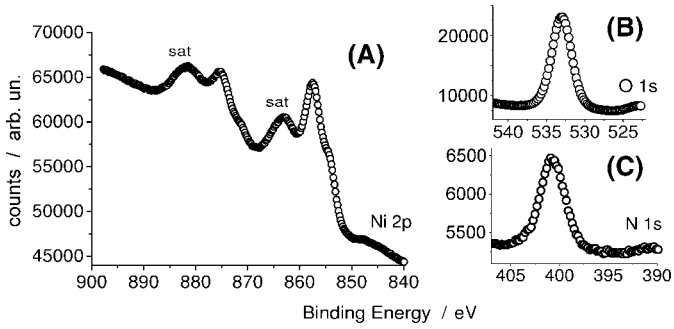

Figure 4. XPS spectra of (A) Ni 2p, (B) O 1s, and (C) N 1s regions, respectively, for the Ni1 sample. The abbreviation "sat" means satellite peaks.

complex surface composition, probably dominated by adsorbed Ni^{2+}(oleate) complexes. Complementary, the N 1s peak, BE = 400 *e*V (fwhm = 2.9 *e*V), can be assigned to the trialkylamine ligand. The quantitative analysis of oxygen/nitrogen gave an 89/11 ratio.

XANES technique provides local information about electronic states and site symmetry of the absorbing atoms. Both XRD and HRTEM data showed that the Ni NPs do not present long-range order and XANES experiments were performed to further address this issue. Figure 5 shows the XANES spectra at the Ni K edge of the Ni2 and Ni7 samples and NiO and Ni standards. The attenuation of the oscillations in the spectra of Ni2 sample confirms a disordered local structure. Corroborating the previous analyses, the annealing process led to an increase of the atomic order in Ni7 sample, as can be verified by the better definition of the oscillations toward the Ni standard (arrows in Figure 5). It is important to emphasize that the XANES region is sensitive not only to interatomic distances but also to angles between atoms, suggesting that different symmetry sites may exist in the NPs. This result is in agreement with the presence of defects and small crystalline domains, as seen by HRTEM, and with the increase of the crystallinity after annealing. The XANES spectra clearly demonstrate that the Ni NPs studied here differ from the metallic nickel or nickel oxides and that they are composed by a complex disordered structure. The XANES spectra also indicate a modification of the p-projected unoccupied density of states compared to the Ni standard, as found in other systems, such as Co NPs.[33] This might be related to the defective sites and/or to surface effects, since the effect is less pronounced in the annealed sample. Simulation of the XANES spectra may help to interpret these features and are expected to be done in the near future.

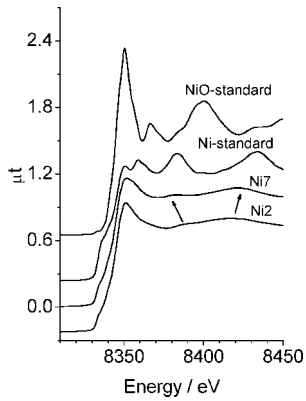

Figure 5. Representative Ni K-edge XANES of Ni2 and Ni7 samples compared to standards.

Magnetic Properties. To verify the magnetic properties of these Ni NPs, we measured the magnetization of the Ni3 sample as function of the temperature. Figure 6 shows the temperature dependence of zero-field-cooled (ZFC) and field-cooled (FC) magnetization of the NPs measured in a small magnetic field (H = 20 Oe). For comparison, a simulated curve for noninteracting superparamagnetic particles of similar size distribution (11.7 ± 0.5 nm) is also presented.[33] In contrast to the ideal superparamagnetic behavior, by decreasing the temperature, the ZFC and FC magnetization curves showed a sharp rise at around 20 K, which resembles a Curie transition. Below this temperature the magnetization exhibited a decrease and ultimately an increase following the behavior of the high-temperature region. This unexpected behavior may be associated to the highly disordered structure of these NPs, which could be related to short-range ferromagnetic coupling among small clusters within each NP. Detail studies about the magnetic properties of these highly disordered NPs have been performed and they will be published elsewhere.

CONCLUSIONS

A method to produce Ni NPs with narrow size distribution in the 4−16 nm range was described in detail and the structural characterization was performed. The Ni NPs exhibit a highly disordered atomic arrangement, shown by HRTEM, the very broad XRD patterns, and the attenuated XANES oscillations. A postsynthesis annealing improved the

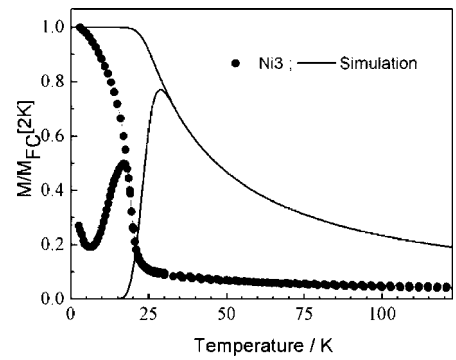

Figure 6. ZFC−FC magnetization curve (points) in terms of magnetic moment per Ni atom for Ni3 sample. The solid line was calculated by considering an ideal noninteracting superparamagnetic NP system and assuming the size distribution obtained by TEM[33] and $K = 5.5 \times 10^4$ erg · cm^{-3} as the Ni effective anisotropy constant.

NP crystallinity. The internal structure may be related to the anomalous magnetic property presented by these NPs, which cannot be described by the conventional superparamagnetic theory. These results emphasize that, regardless of its inherent complexity, the internal structure of NPs is a critical issue to be controlled in the synthesis, and more detailed studies are still necessary for a deep understanding of its influence in the macroscopic properties and applications of transition-metal NPs.

EXPERIMENTAL SECTION

Materials. Reactants were used as received. $Ni(CH_3COO)_2 \cdot 4H_2O$ 99.0% Fluka, *n*-trioctylamine 98%, *n*-tributylamine 98%, *n*-trioctylphosphine 98%, oleic acid 90% and 1,2 dodecanediol 90% were purchased from Aldrich, and *n*-tributylphosphine 99% was obtained from Strem chemicals. Phenylether 99% and anhydrous ethanol were purchased from Aldrich and J.T. Baker, respectively. The $Ni(acac)_2 \cdot 6H_2O$ (acac = acetylacetonate) were prepared from $NiCl_2$ salt and acetylacetone.[34]

NP Synthesis. Nickel NPs of varying sizes (from 4 to 16 nm) were synthesized by adapting procedures described elsewhere.[14,15] Typically, 7 nm Ni NPs were synthesized adding in a 250 mL three-neck round-bottom flask 1.28 mL of oleic acid (4 mmol) and 2.25 mL of *n*-trioctylamine (8 mmol) in a 1 g $Ni(CH_3COO)_2 \cdot 6H_2O$ (4 mmol) solution in 40 mL of phenylether. In a separate flask, 2.1 g of 1,2-dodecanodiol (10 mmol) were dissolved in 10 mL of phenylether. Both reaction vessels were heated up to 80 °C in vacuum for 30 min to remove water from the solvent. In all reactions the temperature ramps were controlled using a Barnant Company temperature controller and type J thermocouple system in contact with the reaction mixture. Heating procedures were conducted typically at a rate of ~3 °C/min.

After removing the water, both mixtures were saturated with N_2 for 15 min, and under a blanket of N_2 the flask containing the Ni^{2+} salt was heated up to 200 °C when 1.2 mL of *n*-trioctylphosphine (4 mmol) was added under vigorous stirring. At this stage the color of solution turned from turquoise to dark green, indicating a chemical transformation due to complexation of *n*-trioctylphosphine to Ni^{2+} and reduction, since *n*-trioctylphosphine can reduce Ni^{2+} to Ni and produce *n*-trioctylphosphine oxide. Then the temperature increased to 220 °C, and before the mixture turned to black, 10 mL of 1,2-dodecanediol solution were rapidly transferred using a 12G × 3'' veterinary needle (Popper & Sons) syringe. In this step, the rapid injection results in a supersaturated solution where the nucleation of the particles occurs. As the Ni NPs nucleate within a short time period, the resulting material exhibits a narrow size distribution. After 3 min of reaction, the solution became deep black as the NPs were formed at the expense of 1,2-dodecanediol. The heating was kept for another 20 min and then the system was left to cool down to room temperature. Finally, ~25 mL of ethanol was slowly added to precipitate the target product, which was separated by centrifugation and kept in vials containing oleic acid/1-buthanol 1:10 O_2-free solution. By keeping the Ni NPs samples under N_2 atmosphere, they can be stored for long periods. By removing the 1-buthanol supernatant, the NPs can be easily dispersed in octane or other nonpolar solvent. Depending on the molar ratio of [ligand]:[Ni^{2+}] the alkyl group and ligand type, the size of the NPs was tuned. The reaction temperature was adjusted in the 200−250 °C range depending on the target NPs. A summary of the reaction conditions are discussed in the Results and Discussion Section. We extended this procedure by substituting the $Ni(CH_3COO)_2 \cdot 4H_2O$ by $Ni(acac)_2 \cdot 6H_2O$ salt that allowed us to prepare Ni NPs with a mean diameter up to 16 nm. Another route was tested,[16,22] where Ni NPs were prepared by injecting 0.162 g of $Ni(acac)_2$ (0.65 mmol) dissolved in 2 mL of *n*-trioctylphosphine (6 mmol) into a reaction vessel containing 8 mL of oleylamine. This mixture was kept at 215 °C, under an N_2 atmosphere, and stirred vigorously. After 30 min the mixture was cooled, and the product was separated, adding 20 mL of ethanol and centrifuging the precipitate. The product was kept in a 10% oleylamine/1-buthanol solution. It is worth mentioning that we fixed the reaction time in 20 min for Ni1 to Ni6 samples while the Ni8 synthesis was held for 30 min, as described in refs 16 and 22. In a complementary experiment (not shown), we extended the refluxing of the Ni2 synthesis up to 60 min to evaluate the effect of the refluxing time in the NP characteristics, and we observed that keeping the synthesis for 20 or 30 min had no significant impact in the mean NPs size.

Annealing. Approximately 300 mg of the Ni2 sample were added to 40 mL of phenylether containing 0.32 mL of oleic acid and 0.5 g of 1,2-dodecanediol. The reaction mixture was heated up to 230 °C and kept for another 30 min. Finally, the material (Ni7) was separated by precipitation with ethanol as described above.

Techniques. TEM and HRTEM images were obtained in a JEOL JEM-3010 microscope (300 kV, 1.7 Å point resolution). TEM samples were prepared by deposition of a 10 μL drop of a $\sim 2g \cdot L^{-1}$ Ni NP octane/octanol/oleic acid (94:5:1) solution on previous prepared amorphous carbon films deposited on copper grids. SAXS measurements were performed at the D11A-SAXS/LNLS beamline ($\lambda = 1.52129$ Å, $q = 0.01-0.32$ Å^{-1}) from $\sim 2g \cdot L^{-1}$ Ni NP octane/octanol/oleic acid (94:5:1) solution. XRD patterns in the $\theta-2\theta$ geometry were measured from powder samples at the D10A-XRD2/LNLS beamline using $\lambda = 1.54982$ Å. XPS spectra were obtained with a Specs, Inc., Phobios, model HSA 3500 150 spherical analyzer and an Al Kα ($E = 1486.6$ eV) source operating at UHV. XANES data were collected at the Ni K-edge at the D04B-XAFS/LNLS beamline from powder samples at 20 K. Magnetization measurements as a function of temperature were performed using Quantum Design.

Acknowledgment. We are in debt to R. Landers for his valuable help in the XPS experiment and analysis. We are grateful to LME-LNLS for the TEM time, and the XPD, XRD2, SAXS, and XAS beamlines at LNLS for the synchrotron techniques. We also thank to the Brazilian agencies CNPq, FINEP, and FAPESP for financial support.

Supporting Information Available: Histograms of size distribution obtained by TEM; SAXS curves of Ni NPs; TEM images of Ni2 and Ni7 (annealed) and corresponding size distribution histograms; additional XRD curves, peak positions, and simulated patterns. This material is available free of charge *via* the Internet at http://pubs.acs.org.

REFERENCES AND NOTES

1. Yin, Y.; Alivisatos, A. P. Colloidal Nanocrystal Synthesis and the Organic-Inorganic Interface. *Nature* **2005**, *437*, 664–670.
2. Neuberger, T.; Scopf, B.; Hofmann, H.; Hofmann, M.; Rechenberg, B. V. Superparamagnetic Nanoparticle for Biomedical Applications: Possibilities and Limitations of a New Drug Delivery System. *J. Magn. Magn. Mater.* **2005**, *293*, 483–496.
3. Schiffrin, D. J. Capped Nanoparticles as Potential Electronic Components with Nanoscale Dimensions. *MRS Bull.* **2001**, *26*, 1015–1019.
4. Wang, X.; Zhuang, J.; Peng, Q.; Li, Y. D. A General Strategy for Nanocrystal Synthesis. *Nature* **2005**, *437*, 121–124.
5. Murray, C. B.; Kagan, C. R.; Bawendi, M. G. Synthesis and Characterization of Mondisperse Nancrystals and Close-Packed Nanocrystal Assemblies. *Annu. Rev. Mater. Sci.* **2000**, *30*, 545–610.
6. Hyeon, T. Chemical Synthesis of Magnetic Nanoparticles. *Chem. Commun.* **2003**, *8*, 927–934.

7. Brust, M.; Kiely, C. J. Some Recent Advances in Nanostructure Preparation from Gold and Silver Particles: A Short Topical Review. *Colloids Surf.* **2002**, *202*, 175–186.
8. Park, J.; Lee, E.; Hwang, N. M.; Kang, M. S.; Kim, S. C.; Hwang, Y.; Park, J. G.; Noh, H. J.; Kini, J. Y.; Park, J. H.; Hyeon, T. One-Nanometer-Scale Size-Controlled Synthesis of Monodisperse Magnetic Iron Oxide Nanoparticles. *Angew. Chem., Int. Ed.* **2005**, *44*, 2872–2877.
9. Green, M. Organometallic Based Strategies for Metal Nanocrystal Synthesis. *Chem. Commun.* **2005**, *24*, 3002–3011.
10. Cheng, G. J.; Puntes, V. F.; Guo, T. Synthesis and Self-Assembled Ring Structures of Ni Nanocrystals. *J. Colloid Interface Sci.* **2006**, *293*, 430–436.
11. Hou, Y.; Kondoh, H.; Ohta, T.; Gao, S. Size-Controlled Synthesis of Nickel Nanoparticles. *Appl. Surf. Sci.* **2005**, *241*, 218–222.
12. Cordente, N.; Amiens, C.; Chaudret, B.; Respaud, M.; Senocq, F.; Casanove, M. J. Chemisorption on Nickel Nanoparticles of Various Shapes: Influence on Magnetism. *J. Appl. Phys.* **2003**, *94*, 6358–6365.
13. Ould-Ely, T.; Amiens, C.; Chaudret, B.; Snoeck, E.; Verelst, M.; Respaud, M.; Broto, J. M. Synthesis of Nickel Nanoparticles. Influence of Aggregation Induced by Modification of Poly(vinylpyrrolidone) Chain Length on Their Magnetic Properties. *Chem. Mater.* **1999**, *11*, 526–529.
14. Murray, C. B.; Sun, S. H.; Doyle, H.; Betley, T. Monodisperse 3d Transition-Metal (Co, Ni, Fe) Nanoparticles and Their Assembly into Nanoparticle Superlattices. *MRS Bull.* **2001**, *26*, 985–991.
15. Murray, C. B.; Sun, S. H.; Gaschler, W.; Doyle, H.; Betley, T. A.; Kagan, C. R. Colloidal Synthesis of Nanocrystals and Nanocrystal Superlattices. *IBM J. Res. Dev.* **2001**, *45*, 47–56.
16. Son, S. U.; Jang, Y.; Park, J.; Na, H. B.; Park, H. M.; Yun, H. J.; Lee, J.; Hyeon, T. Designed Synthesis of Atom-Economical Pd/Ni Bimetallic Nanoparticle-Based Catalysts for Sonogashira Coupling Reactions. *J. Am. Chem. Soc.* **2004**, *126*, 5026–5027.
17. Lamer, V. K.; Dinegar, R. H. Theory, Production and Mechanism of Formation of Monodispersed Hydrosols. *J. Am. Chem. Soc.* **1950**, *72*, 4847–4854.
18. Boyd, P. D. W.; Martin, R. L. Spin−Spin Interactions in Polynuclear Nickel(II) Complexes: Susceptibility and Low-Temperature Magnetization Studies of Tris[bis(pentane-2,4-dionato)nickel(II)]. *J. Chem. Soc., Dalton Trans.* **1979**, *1*, 92–95.
19. Saalfrank, R. W.; Scheurer, A.; Pokorny, K.; Maid, H.; Reimann, U.; Hampel, F.; Heinemann, F. W.; Schunemann, V.; Trautwein, A. X. Trinuclear Oxo-Centered Iron and Iron/Nickel Clusters—Ligand-Controlled Homo−Hetero Valency. *Eur. J. Inorg. Chem.* **2005**, 1383–1387.
20. Cotton, F. A.; Wilkinson, G. *Advanced Inorganic Chemistry - A Comprehensive Text*, 3rd ed.; Interscience Publishers: New York, 1972.
21. Greenwood, N. N.; Earnshaw, A. *Chemistry of the Elements*, 2nd ed.; Elsevier Butterworth-Heinemann: Amsterdam, 2005.
22. Park, J.; Kang, E.; Son, S. U.; Park, H. M.; Lee, M. K.; Kim, J.; Kim, K. W.; Noh, H. J.; Park, J. H.; Bae, C. J.; Park, J. G.; Hyeon, T. Monodisperse Nanoparticles of Ni and NiO: Synthesis, Characterization, Self-Assembled Superlattices, and Catalytic Applications in the Suzuki Coupling Reaction. *Adv. Mater.* **2005**, *17*, 429–434.
23. Jeon, Y.; Lee, G. H.; Park, J.; Kim, B.; Chang, Y. M. Magnetic Properties of Monodisperse NiHx Nanoparticles and Comparison to Those of Monodisperse Ni Nanoparticles. *J. Phys. Chem. B* **2005**, *109*, 12257–12260.
24. Couto, G. G.; Klein, J. J.; Schreiner, W. H.; Mosca, D. H.; de Oliveira, A. J. A.; Zarbin, A. J. G. Nickel Nanoparticles Obtained by a Modified Polyol Process: Synthesis, Characterization, and Magnetic Properties. *J. Colloid Interface Sci.* **2007**, *311*, 461–468.
25. Chen, D. H.; Hsieh, C. H. Synthesis of Nickel Nanoparticles in Aqueous Cationic Surfactant Solutions. *J. Mater. Chem.* **2002**, *12*, 2412–2415.
26. Jeon, Y. T.; Moon, J. Y.; Lee, G. H.; Park, J.; Chang, Y. M. Comparison of the Magnetic Properties of Metastable Hexagonal Close-Packed Ni Nanoparticles with Those of the Stable Face-Centered Cubic Ni Nanoparticles. *J. Phys. Chem. B* **2006**, *110*, 1187–1191.
27. Leite, M. S.; Rodrigues, V.; Zanchet, D. Structural Effects on Au and Ag Colloidal Nanoparticles. *Prog. Colloid Polym. Sci.* **2004**, *128*, 131–134.
28. Zanchet, D.; Hall, B. D.; Ugarte, D. X-ray Characterization of Nanoparticles. In *Characterization of Nanophase Materials*; Wang, Z. L., Ed.; Wiley-VCH: Weinheim, Germany, 1999.
29. Cervellino, A.; Giannini, C.; Guagliardi, A.; Zanchet, D. Quantitative Analysis of Gold Nanoparticles from Synchrotron Data by Means of Least-Squares Techniques. *Eur. Phys. J. B* **2004**, *41*, 485–493.
30. Biju, V.; Khadar, M. A. Electronic Structure of Nanostructured Nickel Oxide Using Ni 2p XPS Analysis. *J. Nanopart. Res.* **2002**, *4*, 247–253.
31. Scofield, J. H. Hartree-Slater Subshell Photoionization Cross-Sections at 1254 and 1487 eV. *J. Electron Spectrosc. Relat. Phenom.* **1976**, *8*, 129–137.
32. Chaubey, G. S.; Barcena, C.; Poudyal, N.; Rong, C. B.; Gao, J. M.; Sun, S. H.; Liu, J. P. Synthesis and Stabilization of FeCo Nanoparticles. *J. Am. Chem. Soc.* **2007**, *129*, 7214–7215.
33. Modrow, H. Tuning Nanoparticle Properties—The X-ray Absorption Spectroscopic Point of View. *Appl. Spectrosc. Rev.* **2004**, *39*, 183–290.
34. Charles, R. G.; Pawlikowski, M. A. Comparative Heat Stabilities of Some Metal Acetylacetonate Chelates. *J. Phys. Chem.* **1958**, *62*, 440–444.